A Fireball and Potentially Hazardous Binary Near-Earth Asteroid (164121) 2003 YT$_1$

Toshihiro Kasuga[1,2] , Mikiya Sato[3], Masayoshi Ueda[3], Yasunori Fujiwara[3], Chie Tsuchiya[1], and Jun-ichi Watanabe[1]

[1] National Astronomical Observatory of Japan, 2-21-1 Osawa, Mitaka, Tokyo 181-8588, Japan; toshi.kasuga@nao.ac.jp
[2] Department of Physics, Faculty of Science, Kyoto Sangyo University, Motoyama, Kamigamo, Kita-ku, Kyoto 603-8555, Japan
[3] The Nippon Meteor Society, Japan

Abstract

We present a fireball detected in the night sky over Kyoto, Japan on UT 2017 April 28 at 15^h 58^m 19^s by the SonotaCo Network. The absolute visual magnitude is $M_v = -4.10 \pm 0.42$ mag. Luminous light curves obtain a meteoroid mass of $m = 29 \pm 1$ g, corresponding to the size of $a_s = 2.7 \pm 0.1$ cm. Orbital similarity assessed by D-criterions (see $D_{SH} = 0.0079$) has identified a likely parent, the binary near-Earth asteroid (164121) 2003 YT$_1$. The suggested binary formation process is a Yarkovsky–O'Keefe–Radzievskii–Paddack-driven rotational disintegration. The asynchronous state indicates the age of $<10^4$ yr, near or shorter than the upper limit to meteoroid stream lifetime. We examine potential dust production mechanisms for the asteroid, including rotational instability, resurfacing, impact, photoionization, radiation pressure sweeping, thermal fracture, and sublimation of ice. We find some of them capable of producing the meteoroid-scale particles. Rotational instability is presumed to cause mass shedding, in consideration of the recent precedents (e.g., asteroid (6478) Gault), possibly releasing millimeter–centimeter scale dust particles. Impacts by micrometeorites with a size $\simeq 1$ mm could be a trigger for ejecting the centimeter-sized particles. Radiation pressure can sweep out the millimeter-sized dust particles, while not sufficient for the centimeter-sized. The other mechanisms are unprovable or unidentified. The feasibility in the parental aspect of 2003 YT$_1$ is somewhat reconciled with the fireball observation, yielding an insight into how we approach potentially hazardous objects.

Unified Astronomy Thesaurus concepts: Solar system astronomy (1529); Meteors (1041); Fireballs (538); Asteroids (72); Near-Earth objects (1092); Meteor radiants (1033); Surveys (1671); Catalogs (205); Micrometeoroids (1048)

Supporting material: machine-readable tables

1. Introduction

The worldwide meteor survey networks have established the procedure for identifying meteoroid orbits in streams and associated parent bodies, asteroids, and comets, mostly known as near-Earth objects (NEOs; SonotaCo 2009; Rudawska & Jenniskens 2014; Ye et al. 2016; Jenniskens 2017). Some NEOs, meteorite falls, and fireballs have been linked with potentially hazardous asteroids (PHAs; Madiedo et al. 2013, 2014; Svetsov et al. 2019) of which the Taurids are studied in many cases (Brown et al. 2013; Olech et al. 2017; Spurný et al. 2017; Clark et al. 2019). Physical disintegration of NEOs result in producing orbit-hugging dust (streams) which may cross Earth's orbit. Suggested mechanisms, especially for those of asteroids, include rotational instability, thermal stress, collisions (impacts), and so on (Jewitt 2012; Jewitt et al. 2015). Asteroidal stream parents should be, or used to be, losing mass while among the few mass-loss activities other than activity driven by sublimation of ice are identified (Kasuga & Jewitt 2019).

A relatively slow, bright fireball was detected in the sky over Kyoto, Japan on UT 2017 April 28 at 15^h 58^m 19^s through the SonotaCo Network (SonotaCo 2009). The small semimajor axis ($a = 1.111$ au) and high inclination ($i = 43°.9$) present its peculiar orbit. The dynamical properties, as given by orbit-linking D-criterions (see Southworth & Hawkins 1963), find a close association with the near-Earth asteroid (NEA) (164121) 2003 YT$_1$ (hereafter, 2003 YT$_1$; see details in Section 3). The short distance from the asteroid orbit to Earth's orbit (see 0.0026 au at the descending node) is compatible with those of

meteoroid streams for showers ($\lesssim 0.01$ au; Vaubaillon et al. 2019), suggesting that both the fireball and 2003 YT$_1$ practically cross Earth's orbit. This asteroid–meteor pair is likely to be secured, giving a rare opportunity for understanding of meteoroid production.

The NEA 2003 YT$_1$ was discovered on UT 2003 December 18 in the course of the Catalina Sky Survey (Tichy et al. 2003). Based upon the absolute magnitude of $H = 16.2$ and the low minimum orbit intersection distance (MOID) of ~ 0.003 au (NASA/Jet Propulsion Laboratory (JPL) Small-Body Database), the object is a PHA (Larson et al. 2004; Hicks et al. 2009). The impact probability to Earth is calculated as $\sim 6\%$ per 10^7 yr (Galiazzo et al. 2017). The Arecibo radar delay-Doppler and optical photometric observations independently identified 2003 YT$_1$ has a binary system (Nolan et al. 2004a). The suggested formation process is a rotational instability, a breakup/fission driven by Yarkovsky–O'Keefe–Radzievskii–Paddack (YORP) torques (Pravec & Harris 2007). The primary has 1.1 ± 0.2 km in diameter (D_p) and the secondary with a diameter of 0.21 ± 0.06 km (D_s), having a distance of 2.7 km (Nolan et al. 2004b). The primary's rotation period is 2.343 ± 0.001 hr, and the light-curve amplitude of ~ 0.16 mag exhibits its nearly spheroidal shape (Galád et al. 2004; Larson et al. 2004; Warner et al. 2018). The secondary's rotation period of $\lesssim 6$ hr and its orbital period of ~ 30 hr (eccentric orbit) suggest the asynchronous state (Nolan et al. 2004a, 2004b). Geometric albedos (in visual and infrared) are measured by thermal infrared observations, $p_v = 0.24 \pm 0.16$ from the ground-based (Delbo et al. 2011), and $p_v = 0.20 \pm 0.10$ and $p_{IR} = 0.33 \pm 0.14$ from the space (*Wide-field Infrared Survey*

Explorer (*WISE*)/NEOWISE; Mainzer et al. [2012]). Near-infrared spectra (0.7–2.5μm) reveal the surface assemblage dominated by orthopyroxene with any lack of olivine content on 2003 YT$_1$, implying a taxonomic V-type asteroid (Abell et al. [2004], [2005]; Sanchez et al. [2013]). The regolith breccia (<25μm in size mostly; Ieva & Dotto [2016]) could be originated in a larger, extensive-igneous processed precursor body (howardites, eucrites, and diogenites-assemblage, HED). The V-type NEAs (Cruikshank et al. [1991]) remain an open question for their origin (from (4) Vesta?; Cochran et al. [2004]; Burbine et al. [2009]).

In this paper we present the orbital and physical properties of the Kyoto fireball taken by the SonotaCo Network, including the trajectory, radiant point, geocentric velocity, orbit, and meteoroid mass (size) and further discuss the possible relation to the parental binary NEA 2003 YT$_1$ by examining its potential dust production mechanisms.

2. SonotaCo Network

The fireball studied here is from the SonotaCo Network database. Automated multi-station video observations use more than 100 cameras at 27 sites in Japan (SonotaCo [2009]).[4] The database is advantaged in the similar type of camera setup of all the network sites. The CCD cameras are mostly WATEC series with $f = 3.8$–12 mm lens having a field of view (FOV) $\approx$ 30°–90°. The video format is digitized in 720×480 or 640×480 pixels audio video interleave (AVI) from the National Television System Committee (NTSC) signal (29.97 frames per second, interlaced), and the video field with a time resolution of $\simeq 0.017$ s (1/59.94 s) is used for measurement. Meteors are detected by UFOCaptureHD2 software, and the data reductions and orbit determinations are conducted by UFOAnalyzerV2 and UFOOrbitV2, respectively. Limiting magnitude for multi-station observations is estimated to be apparent magnitude $<+3$ and absolute magnitude $<+2$ for each (SonotaCo [2009]).

The database includes orbital and physical parameters of meteors, such as trajectory (apparent position on the sky plane), radiant point, geocentric velocity, orbital elements, brightness (magnitude), and height above sea level.[5] Astrometry and photometric calibrations for meteors are conducted using field stars in the background and the SKY2000 Master Catalog, Version 4 (Myers et al. [2001]) installed in the UFOAnalyzerV2. Single-station observation has some uncertainties of measurements but are negligibly small, as estimated by the position in the sky plane $\sim 0°.03$ (SonotaCo [2009]), distance to meteor $\lesssim 200$ m, and elevation angle $\sim 0°.02$–0°.03. Lens distortion is corrected by background stars' positions fitted by a polynomial equation. The aperture radius used for the stars is 5 pixels in the image ($\sim 0°.5$) and the sky background is determined within a concentric annulus having projected inner and outer radii of 5 pixels and 7.5 pixels ($\approx 0°.5 \sim 0°.7$), respectively. For meteors on the other hand, the aperture sets a minimum rectangle that covers the total brightness of a meteor including its tail, and the sky background was subtracted by the field prior to the meteor appearance. More than five background stars are used to count the flux of the meteor. Then we obtain apparent magnitude of the meteor, $m(\text{obs})$. The photometric uncertainty (mag) is estimated from the typical uncertainty of

comparison stars, ~ 0.5 mag, and the correction for the saturated apparent magnitude of meteor is expressed as

$$\sqrt{0.5^2 + (m(\text{obs})' - m(\text{obs}))^2}, \qquad (1)$$

where $m(\text{obs})'$ is the corrected apparent magnitude. The $m(\text{obs})'$ is derived from $m(\text{obs})' = m(\text{obs}) + k(m(\text{obs}))^2$, where $m(\text{obs}) < 0$ and $k = -0.03$. Details of the analysis procedure is described in the UFOAnalyzerV2 manual,[6] and private communication with SonotaCo.

3. Results

The fireball trajectory and observing sites (ID[7]) are shown in Figure [1]. The images of the fireball are represented in Figure [2]. This event was simultaneously detected at 11 sites with 12 cameras. The data sets taken at Tokyo (TK8_S7) and Osaka (Osaka03_3N) have imaged the most part of trajectory, from the beginning to the end. The numbers of video fields that have acquired the fireball position and brightness are 159 out of 173 in the Tokyo data and 194 out of 204 in the Osaka data, respectively. Therefore these two data sets are primarily used for orbit determinations and photometric measurements. Orbital results are listed in Tables [1]–[3]. Photometric results are given in Tables [4] and [5].

3.1. D-criterions

We searched dynamical similarities between the fireball and asteroids using distances defined in the orbital elements space, *D*-criterions, by comparing a (semimajor axis), e (eccentricity), i (inclination), q (perihelion distance), ω (argument of perihelion), and Ω (longitude of ascending node; Williams et al. [2019]). Three types of *D*-criterions are used to reduce biases therein. The first one is D_{SH} (Southworth & Hawkins [1963]) depending mostly on q, the second is D' (Drummond [1981]) depending mostly on e, and the third is D_{ACS} (Asher et al. [1993]) neutralizing rapid evolutions of the ω and Ω with time (see Dumitru et al. [2017]). A smaller D indicates a closer degree of orbital similarity between two bodies. By comparing with the orbit of 2003 YT$_1$ (see Table [3]), we find more than one order of magnitude smaller values than the significant empirical threshold (e.g., $D_{\text{SH}} \lesssim 0.10$–0.20; Williams et al. [2019]). The close-knit orbit interprets that 2003 YT$_1$ is a possible parent body. Results are shown in Table [6].

We further searched other probable meteors having the similar orbits from the SonotaCo data sets in 2007–2018 and the European video Meteor Network Database (EDMOND;[8] Kornoš et al. [2014a], [2014b]) in 2001–2016, but found few compelling cases (Appendix [A]).

3.2. Meteoroid Mass

For initial meteoroid mass, the classical meteor luminous model (Bronshten [1983]; Ceplecha et al. [1998]) has been used but with non-negligible uncertainty in the ablation coefficient. Instead, we have made a new meteor luminous model as described in Appendix [B].

---

[4] As of 2018; http://sonotaco.jp/doc/SNM/2018A.txt.
[5] http://sonotaco.jp/doc/SNM/index.html

[6] http://sonotaco.com/soft/download/UA2Manual_EN.pdf
[7] Here we note in the ID that is an assignment for the observing site. Take TK8_S7 (Tokyo data) for example, the location is expressed as TK8 and the underscore S7 is named after the camera.
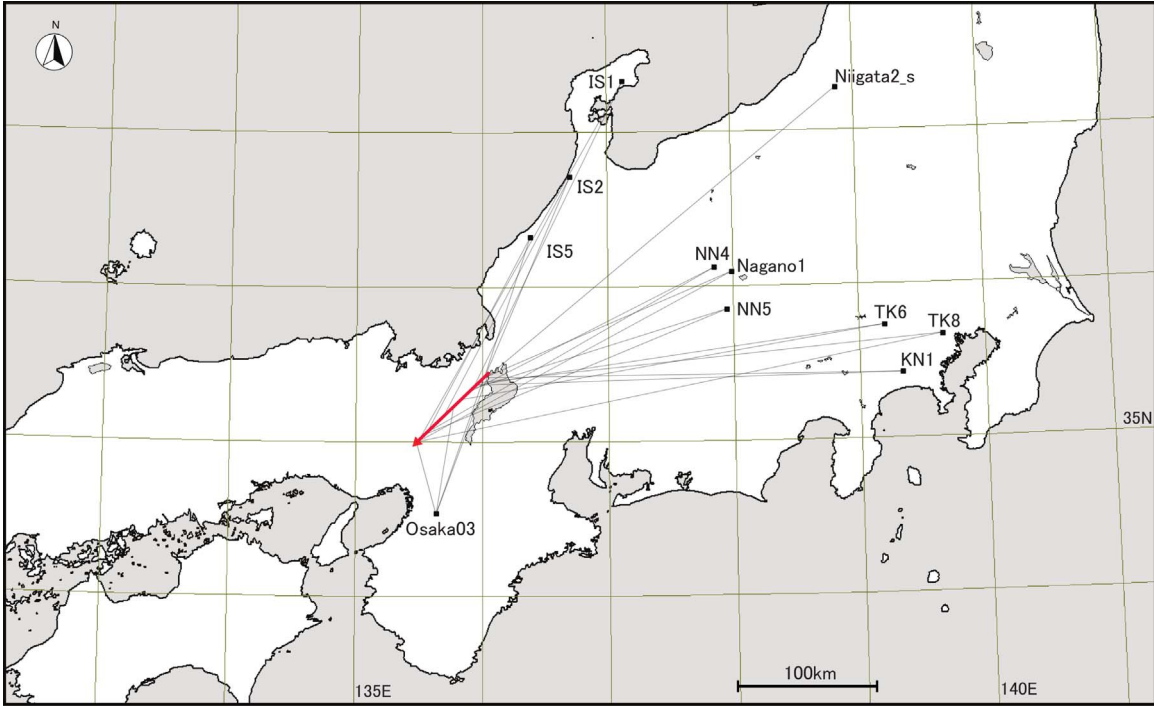[8] http://www.daa.fmph.uniba.sk/edmond

Figure 1. Map showing the projection of the fireball atmospheric trajectory (red arrow), including 11 observation sites (ID) and the lines of sight (thin line). The direct distance of the trajectory is approximately 70 km. The ID is listed in http://sonotaco.jp/doc/SNM/2017C.txt. ©SonotaCo.

The total mass of the meteoroid (source of fireball), m(g), can be estimated from the light curves (Figure 3) using the new luminous model (Equation (18)), which is given by

$$m = \sum_N \left[\frac{2I}{\tau v^2} \left(\frac{2}{\sigma v^2} - 1 \right)^{-1} \int_0^t dt \right]_N, \quad (2)$$

where N is the number sign of the video field (see Tables 4 and 5), I is the meteor luminosity, τ is the luminous efficiency, v is the meteor velocity (cm s^{-1}), σ is the ablation coefficient (s^2 km^{-2}), and t is the time (s). We define the meteor luminosity in visual magnitude-based units as $I = 10^{-0.4M_v}$, where M_v is the absolute magnitude (as seen from distance of 100 km).

The luminous efficiency, τ, is the fraction of a meteoroid's instantaneous kinetic energy loss converted into light in a particular bandpass. The uncertainty within is substantial (0.05 ∼ 10 s%) as it depends on many factors, e.g., the speed, mass, composition of meteoroid and the height at which it ablates (different flow regimes), and the spectral sensitivity of the detector (see Weryk & Brown 2013; Subasinghe & Campbell-Brown 2018; see the review in Popova et al. 2019). For this study, we use the velocity dependence (Table 1 in Ceplecha & McCrosky 1976) considering the performance of CCD cameras (e.g., low resolution). Setting $v = 23.7$ km s^{-1} finds $\tau = 5 \times 10^{-13}$ erg^{-1} s 0 mag. The τ-value corresponds to 0.75% efficiency. The conversion is given by multiplying 1.5×10^{10} erg s^{-1} 0 mag^{-1}, i.e., the luminous energy equivalent to zero magnitude in visual (Table 6 in Ceplecha et al. 1998).

The critical bulk density, ρ, for the meteoroid and 2003 YT$_1$ is estimated. An asteroid shape is approximated as an ellipsoid with axes $a \geqslant b = c$, in rotation about the c-axis. A limit to the ratio of the equatorial axes is $f = a/b = 10^{0.4\Delta m}$, where Δm is

Table 1
Kyoto Fireball Trajectory

	Longitude (deg E)	Latitude (deg N)	Height (km)
Beginning	136.0156 ± 0.0004	35.4275 ± 0.0005	88.80 ± 0.07
End	135.4746 ± 0.0002	34.9859 ± 0.0003	47.80 ± 0.04

Note. The atmospheric trajectory for the fireball (UT 2017 April 28) are determined by five camera measurements. The observing IDs are TK8_S7, Osaka03_3N, Osaka03_06 (the location: Osaka03 obtained the fireball data with two cameras which are expressed as Osaka03_3N and Osaka03_06, respectively.), IS2_S, and IS5_SW (see Figure 1). The orbital properties (e.g., the elements), speed, and positioning accuracy (see Section 2) give the estimation of the uncertainties.

the light-curve amplitude. Rotation around the c-axis with period, P_{rot}, gives a condition that the gravitational acceleration is greater than the centripetal acceleration which is the largest at the top of the shape. The net acceleration toward the center of a rotating object is >0, giving the relation as (Equation (4) of Jewitt & Li 2010)

$$\rho > \left(\frac{3\pi}{GP_{rot}^2} \right) \left(\frac{a}{b} \right)^2, \quad (3)$$

where G is the gravitational constant. We substitute $G = 6.67 \times 10^{-11}$ m^3 kg^{-1} s^{-2}, $P_{rot} = 2.343$ hr, $\Delta m = 0.16$ mag (i.e., $f = a/b = 1.16$) into Equation (3), then obtain $\rho \gtrsim 2700$ kg m^{-3}. This is consistent with the lower limit for rubble pile asteroids with diameters of 0.3–10 km ($\rho = 2.7$ g cm^{-3}), as formulated by the observed light-curve amplitude versus spin rate (Pravec 2005). The proposed bulk density of 2010 ± 700 kg m^{-3} (Brooks 2006) may be uncertain due to the

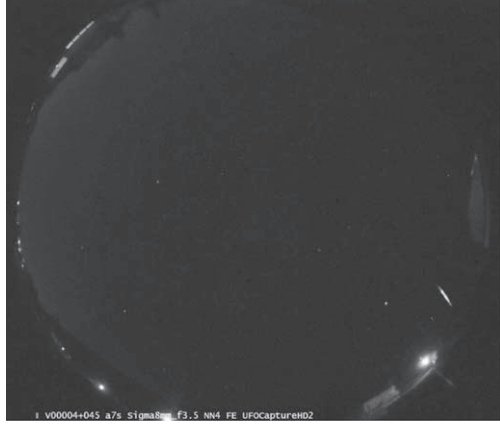(a) Composite image, with 204 fields (3.40 sec): Watec (WAT-231S2), f=3 mm, F0.95 and FOV= 94°×68° at Osaka (Osaka03_3N).

(b) The 173 fields (2.89 sec): Watec (WAT-100N), f=8 mm, F0.8 and FOV= 45°×34° at Tokyo (TK8_S7).

(c) The 164 fields (2.74 sec): Watec, f=6 mm, F1.2 and FOV= 57°×43° at Ishikawa (IS5_SW).

(d) The 162 fields (2.70 sec): Watec (WAT-100N), f=3.8 mm, F0.8 and FOV= 89°×69° at Ishikawa (IS1).

(e) The 104 fields (1.74 sec): Sony α7s (High-definition 1920×1080 pixel, 60i, interlaced), f=8 mm, F3.5 and fish-eye lens at Nagano (NN4_FE).

(f) The 41 fields (0.68 sec): Watec (WAT-100N), f=6 mm, F0.8 and FOV= 57°×43° at Tokyo (TK6_w).

Figure 2. Composite images of the fireball recorded on UT 2017 April 28 at $15^{\rm h}\,58^{\rm m}\,19^{\rm s}$. The number of detected video fields (duration time): camera, focal length (f), F-number, and FOV at observation site (ID). The date and time within the image is in JST.

assumption of the circular orbit of the secondary. The orbit is actually eccentric ($e \simeq 0.18$; Fang & Margot 2012; see Pravec et al. 2016).

Substituting $v(=v_{\rm g}) = 2.37 \times 10^6 \,{\rm cm\,s^{-1}}$, $\tau = 0.75\%$, $\sigma = 0.0017 \,{\rm s^2\,km^{-2}}$ (Appendix B) and $t = 0.017$ s into Equation (2),

we obtain m (see Tables 4 and 5). The weighted mean of the total mass is $m = 29 \pm 1$ g, corresponding to the meteoroid size of $a_{\rm s} = 2.7 \pm 0.1$ cm for $\rho = 2700 \,{\rm kg\,m^{-3}}$. For reference, the classical luminous model (Equation (11)) is applied too. The resulting masses are compared in Table 7.

Table 2
Radiant Point and Geocentric Velocity

Object	α[a] (deg)	δ[b] (deg)	v_g[c] (km s^{-1})	Δr[d] (au)	λ_s[e] (deg)	UT Date
Fireball	321.2 ± 0.5	$+51.2 \pm 0.3$	23.7 ± 0.5	...	38.3150	2017 Apr 28.7
2003 YT$_1$	320.54	+50.97	23.7	0.0026	38.3333	2017 Apr 28.7
	87.30	-36.10	23.7	0.0279	218.3331	2017 Oct 31.8

Notes. Radiant point and geocentric velocity of 2003 YT$_1$ are calculated by the parallel shift of moving vector at each orbital node (method (P) in Neslusan et al. 1998). The descending node is at $\lambda_s = 38°.3333$ (2017 April 28.7) and the ascending node is at $\lambda_s = 218°.3331$ (2017 October 31.8).
[a] R.A. (J2000.0).
[b] Decl. (J2000.0).
[c] Geocentric velocity.
[d] Distance from descending/ascending node to Earth's orbit.
[e] Solar longitude (J2000.0).

Table 3
Orbital Elements and Period

Object	a[a] (au)	e[b]	i[c] (deg)	q[d] (au)	ω[e] (deg)	Ω[f] (deg)	P_{orb}[g] (yr)
Fireball	1.111 ± 0.016	0.297 ± 0.004	43.9 ± 0.9	0.781 ± 0.007	91.2 ± 2.7	38.315 ± 0.001	1.17
2003 YT$_1$	1.110	0.292	44.1	0.786	91.0	38.335	1.17

Notes. The uncertainties are propagated from those of radiant point and geocentric velocity (Table 2) through the Monte Carlo technique. Orbital data of 2003 YT$_1$ are obtained from NASA JPL Small-Body Database Browser (2018).
[a] Semimajor axis.
[b] Eccentricity.
[c] Inclination.
[d] Perihelion distance.
[e] Argument of perihelion.
[f] Longitude of ascending node.
[g] Orbital period.

4. Discussion

Here, we recapitulate the binary formation process of 2003 YT$_1$ and evaluate possible dust production mechanisms for millimeter–centimeter scale particles.

4.1. Binary Formation

The 2003 YT$_1$ binary system is presumed to be formed from a breakup/fission by rotational instability with YORP spin-up. The primary with $D_p \lesssim 10$ km and the normalized total angular momentum of the binary system α_L[9] = 1.13 suggest that the 2003 YT$_1$ binary system was formed from a precursor body spinning at the critical rate, resulting in fission and mass shedding (Group A in Table 1 and Figures 2 and 3 from Pravec & Harris 2007; reviewed in Margot et al. 2015; Walsh & Jacobson 2015). The 2003 YT$_1$ primary rotates (P_{rot} = 2.343 hr) closely to the spin barrier period of ~2.2 hr (Warner et al. 2009; Chang et al. 2015). This can reasonably lead to a rotational breakup when centrifugal forces have exceeded the gravitational and cohesive forces (Pravec et al. 2008).

We calculate the YORP timescale of the spin, τ_Y, using the ratio of the rotational angular momentum, L, to the torque, T.
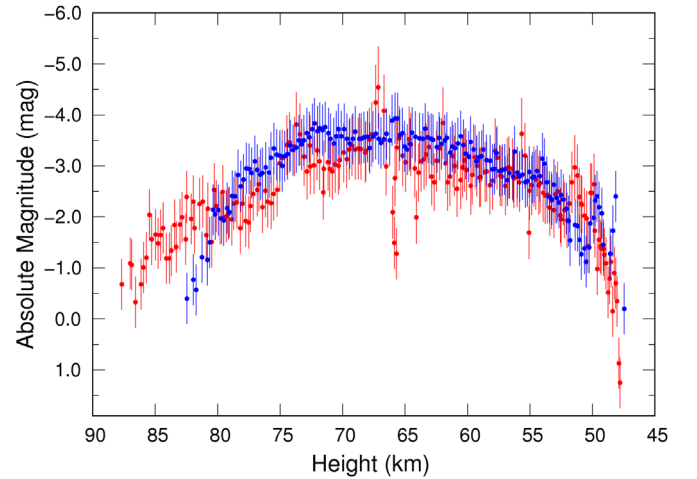

Figure 3. Light curves of the fireball measured at Tokyo (blue) and Osaka (red). Absolute magnitudes as a function of height are plotted from Tables 4 and 5. The weighted mean of maximum brightness is -4.10 ± 0.42 mag. The uncertainty of height is within the circle.

The relation is given by Jewitt et al. (2015) as

$$\tau_Y \sim K D_e^2 R_h^2, \qquad (4)$$

where K is a constant, D_e is the asteroid diameter (kilometer), and R_h is the heliocentric distance (astronomical unit). The value of constant K is experimentally estimated from published

---

[9] The α_L is the ratio of the total angular momentum of the system to the angular momentum of a critically spinning spherical body. The spherical body is comprised of the mass and volume equivalent to the two objects of the binary system. The internal friction angle is $90°$ (Pravec & Harris 2007).

Table 4
Tokyo Data (ID: TK8_S7)

N	H^a	$L_D{}^b$	$m(obs)^c$	$M_v{}^d$	I^e	$m_N{}^f$
1	82.46 ± 0.12	351.1	2.33 ± 0.50	−0.40 ± 0.50	1.45 ± 0.67	0.016 ± 0.007
2	81.95 ± 0.12	351.6	1.96 ± 0.50	−0.77 ± 0.50	2.03 ± 0.94	0.023 ± 0.011
3	81.72 ± 0.12	351.8	2.16 ± 0.50	−0.57 ± 0.50	1.69 ± 0.78	0.018 ± 0.008
4	81.25 ± 0.12	352.3	1.52 ± 0.50	−1.21 ± 0.50	3.05 ± 1.40	0.034 ± 0.016
5	80.82 ± 0.12	352.8	1.58 ± 0.50	−1.16 ± 0.50	2.91 ± 1.34	0.032 ± 0.015
6	80.63 ± 0.12	353.0	1.24 ± 0.50	−1.50 ± 0.50	3.98 ± 1.83	0.044 ± 0.020
7	80.37 ± 0.12	353.2	0.60 ± 0.50	−2.14 ± 0.50	7.18 ± 3.31	0.079 ± 0.036
8	80.20 ± 0.12	353.4	0.69 ± 0.50	−2.05 ± 0.50	6.61 ± 3.04	0.073 ± 0.034
9	79.95 ± 0.12	353.7	0.61 ± 0.50	−2.13 ± 0.50	7.11 ± 3.28	0.079 ± 0.037
10	79.68 ± 0.12	353.9	0.77 ± 0.50	−1.97 ± 0.50	6.14 ± 2.83	0.068 ± 0.031

Notes. Total mass $m = 31 ± 1$ g is the sum of m_N. The maximum brightness is $M_v = −3.93 ± 0.50$ mag.
[a] Height above sea level (km).
[b] Distance to meteor (km). The uncertainty on each measurement is $\lesssim 0.2$ km.
[c] Apparent magnitude. The uncertainty is from Equation (1).
[d] Absolute magnitude.
[e] Meteor luminosity in visual magnitude-based units.
[f] Mass measured on video field N (g). The duration time is 0.017 s.

(This table is available in machine-readable form.)

Table 5
Osaka Data (ID: Osaka03_3N))

N	H^a	$L_D{}^b$	$m(obs)^c$	$M_v{}^d$	I^e	$m_N{}^f$
1	87.67 ± 0.07	135.4	−0.02 ± 0.50	−0.68 ± 0.50	1.87 ± 0.86	0.021 ± 0.010
2	87.00 ± 0.07	134.2	−0.45 ± 0.50	−1.09 ± 0.50	2.73 ± 1.26	0.030 ± 0.014
3	86.88 ± 0.07	134.0	−0.42 ± 0.50	−1.06 ± 0.50	2.65 ± 1.22	0.029 ± 0.014
4	86.58 ± 0.07	133.4	0.30 ± 0.50	−0.33 ± 0.50	1.36 ± 0.62	0.015 ± 0.007
5	86.13 ± 0.07	132.6	−0.07 ± 0.50	−0.68 ± 0.50	1.87 ± 0.86	0.021 ± 0.010
6	85.94 ± 0.07	132.3	−0.40 ± 0.50	−1.01 ± 0.50	2.54 ± 1.17	0.028 ± 0.013
7	85.70 ± 0.07	131.8	−0.60 ± 0.50	−1.20 ± 0.50	3.02 ± 1.39	0.034 ± 0.016
8	85.46 ± 0.07	131.4	−1.45 ± 0.50	−2.04 ± 0.50	6.55 ± 3.01	0.072 ± 0.033
9	85.28 ± 0.07	131.1	−0.97 ± 0.50	−1.56 ± 0.50	4.21 ± 1.94	0.047 ± 0.022
10	84.97 ± 0.07	130.5	−1.07 ± 0.50	−1.65 ± 0.50	4.57 ± 2.10	0.050 ± 0.023

Notes. Total mass $m = 26 ± 1$ g is the sum of m_N. The maximum brightness is $M_v = −4.54 ± 0.80$ mag.
[a] Height above sea level (km).
[b] Distance to meteor (km). The uncertainty on each measurement is $\lesssim 0.2$ km.
[c] Apparent magnitude. The uncertainty is from Equation (1).
[d] Absolute magnitude.
[e] Meteor luminosity in visual magnitude-based units.
[f] Mass measured on video field N (g). The duration time is 0.017 s.

(This table is available in machine-readable form.)

measurements of YORP acceleration in seven well-characterized asteroids (Table 2 from Rozitis & Green 2013). Scaling K to the bulk density of primary $\rho = 2700$ kg m^{-3} and its rotation period $P_{rot} = 2.343$ hr, we find $K \sim 5 \times 10^{13}$ s km^{-2} au^{-2}. By Equation (4), the primary with $D_e(=D_p) = 1.1$ km orbiting at $R_h \sim 1.11$ au takes $\tau_Y \sim 2$ Myr. This is consistent with the previous study (~ 1 Myr; Vokrouhlický et al. 2015) and much shorter than the catastrophic collisional lifetime for 1 km NEAs (~ 100 Myr, Bottke et al. 1994; see also Section 4.2.3). The YORP spin-up plays a contributory role.

The cohesive strength is a required parameter for asteroids rotating near or faster than the spin barrier to resist rotational forces (Scheeres et al. 2010). The strength at a rotational breakup of a body is estimated by $S_c \sim \rho(D_s/D_p)(\Delta v)^2$ (Equation (5) of Jewitt et al. 2015), where D_p and D_s are the

dispersed fragmental sizes of the primary and secondary, respectively, Δv is the excess velocity of escaping fragments, assumed comparable to the escape velocity (v_e) from the primary, and ρ is the bulk density. With the same value for ρ (see Section 3.2) and substituting $(D_s/D_p) = 0.19$ (the diameter ratio of the secondary to primary), and $\Delta v (=v_e) = 0.68$ m s^{-1}, we find $S_c \sim 240$ N m^{-2}. This value is comparable to weak, van der Waals forces (~ 10–100 N m^{-2}) bounded in a modeled rubble pile asteroid (Scheeres & Sánchez 2018), while $10^5 \times$ weaker than those of competent rocks (10^7–10^8 N m^{-2}). Therefore, given a rubble pile structure, a rotational breakup/fission is a probable process for the 2003 YT$_1$ binary formation.

The breakup/fission period is inferred from the spin asynchronous state of the 2003 YT$_1$ binary system in the present day. The timescale from asynchronous to synchronous state, τ_{sync}, limits to the age of the binary system. Two models

Table 6
D-criterions

Criterion	Value	Source
D_{SH}	0.0079	(1)
D'	0.0091	(2)
D_{ACS}	0.0061	(3)

Note. (1) Southworth & Hawkins (1963), (2) Drummond (1981), (3) Asher et al. (1993).

Table 7
Mass Comparison

Data	Classical Model[a]	New Model[b]
Tokyo	11 ± 1 g	31 ± 1 g
Osaka	9 ± 1 g	26 ± 1 g
...	10 ± 1 g [c]	29 ± 1 g [c]

Notes.
[a] Equation (11) (e.g., Ceplecha et al. 1998).
[b] Equation (18) from this work.
[c] The weighted mean of measurements.

are applied for 2003 YT$_1$ using the data of known synchronous binary asteroid systems (Table 3 in Fang & Margot 2012). One estimates $\tau_{sync} = 10^{7-8}$ yr by the tidal Love number proportional to the radius (Goldreich & Sari 2009), another estimates $\tau_{sync} = 10^{4-5}$ yr by the tidal Love number inversely proportional to the radius (Jacobson & Scheeres 2011). The former just agrees with the large-sized binaries having a primary with $D_e \sim 4$ km; on the other hand, the latter fits well for smaller-sized objects too (down to $D_e \sim 0.4$ km). For 2003 YT$_1$ we thus take $\tau_{sync} = 10^{4-5}$ yr (Fang & Margot 2012). The interpretation is that this binary is of an age of $<10^4$ yr, comparable with the upper limit of the meteoroid stream lifetime, $<10^4$ yr (Jenniskens & Lyytinen 2005).

Another example is proposed by the small-sized V-type NEA pair ($D_e \sim 25$–50 m) also having the young age of separation $<10^4$ yr ($D' = 0.0035$ for 2017 SN$_{16}$ and 2018 RY$_7$; Moskovitz et al. 2019). The YORP-driven breakups for the (sub)kilometer-sized bodies may suggest moderately recent events.

4.2. Dust Production Mechanisms

We look into possible dust production mechanisms from 2003 YT$_1$. The consequences of YORP-driven breakups are reported from the (sub)kilometer-sized main-belt asteroids, as exampled by P/2010 A2 (Jewitt et al. 2010, 2013; Agarwal et al. 2013), P/2013 R3 (Jewitt et al. 2014a, 2017; Hirabayashi et al. 2014), and (6478) Gault (Chandler et al. 2019; Hui et al. 2019; Jewitt et al. 2019b; Kleyna et al. 2019; Moreno et al. 2019; Ye et al. 2019). Additionally, other different mechanisms may work together, e.g., impact for P/2010 A2 and outgassing torques from sublimated ice for P/2013 R3 (Jewitt et al. 2015). Here, we estimate breakup/fission (rotational instability), resurfacing, impact, thermal fracture, photoionization, radiation pressure sweeping, and sublimation of water ice.

4.2.1. Breakup/Fission (Rotational Instability)

Binary NEAs show a trend of having large values of thermal inertia, $\Gamma \gtrsim 400$ J m^{-2} s$^{-0.5}$ K^{-1}, typically twice those of non-binary NEAs, suggesting that the fine regoliths were swept away during the YORP-induced binary formation (Walsh et al. 2008; Delbo et al. 2011). For 2003 YT$_1$, it would be difficult to determine the sizes and speeds of released dust particles at the presumed breakup time, whereas the measured values of the recent precedents infer the large particles (millimeter–centimeter scale) with nearly the gravitational escape speeds $\lesssim 1$ m s^{-1} (see $a_s = 6$ mm–40 cm from P/2010 A2, ~ 1 cm from P/2013 R3, and $\lesssim 1$ cm from Gault; Jewitt et al. 2013, 2014a, 2019b). On the process, resurfacing could be partly involved (Gault; Marsset et al. 2019). A similar situation might be expected for 2003 YT$_1$. The dust particles are, if released, supposed to reach the Earth within the typical stream lifetime (10^4 yr). The short distance to Earth's orbit, e.g., $\Delta r = 0.0026$–0.0279 au (Table 2), may help. Accordingly, the rotational breakup/fission ejecting the millimeter–centimeter scale dust particles is considered as a likely cause.

4.2.2. Resurfacing

Planetary encounters, space weathering, and thermal processes could induce resurfacing, which might lose dust particles on the surfaces to some extent. For example, the timescale for Q-type NEAs to be refreshed into S-type (at 1 and $q \lesssim 0.9$ au) is estimated to be 10^{5-7} yr by planetary encounters (Binzel et al. 2010; Nesvorný et al. 2010), space weathering (Graves et al. 2018), and thermal processes (Graves et al. 2019). For V-type NEAs, the aftermath of those processes are unclear (space weathering; Pieters et al. 2012; Fulvio et al. 2016), while the timescale of resurfacing itself seems to be 10–1000 times longer than the typical stream lifetime. The resurfacing is thus unlikely to be responsible for releasing the source of meteors.

4.2.3. Impact

Impacts can cause catastrophic disruption of asteroids and/or dust production. The catastrophic disruption is defined as the impact resulting in losing a half of the target's mass. The specific impact energy threshold is expressed as $Q_D^* = (1/2)(D_i/D_t)^3 \Delta V_{NEA}^2$, where D_i, D_t, and ΔV_{NEA} are the size of the impactor and the target (an assumed precursor body) and the relative velocity among NEAs, respectively (Jutzi et al. 2010). With $Q_D^* \sim 1400$ J kg^{-1} for catastrophic disruptions of stone meteorites (Flynn & Durda 2004; Flynn et al. 2018), $D_t \approx D_p = 1100$m (assuming the primary size occupying $>80\%$ of the precursor body) and $\Delta V_{NEA} = 17$–20 km s^{-1} (Bottke et al. 1994; Jeffers et al. 2001), we find $D_i \sim 20$ m. This catastrophic event is inferred from the interval between impacts, τ_{col} (Davis et al. 2002), as

$$\tau_{col} \simeq \frac{4}{\pi (D_t + D_i)^2 \, P_{NEA} \, N_i(\geqslant D_i)}, \tag{5}$$

where P_{NEA} is the collision frequency per unit area in the near-Earth region (km^{-2} yr^{-1}), and $N_i(\geqslant D_i)$ is the cumulative number of impactor larger than D_i. The NEA cumulative size distribution is measured by *WISE/NEOWISE*, $N_i(D_i \geqslant 140$ m$) \simeq 13{,}200 \times (140$ m$/D_i)^{1.32}$ (Mainzer et al. 2011), and we presumably extend the equation down to 20 m in diameter. With $D_i \sim 20$ m, $N_i(\gtrsim 20$ m$) \sim 1.7 \times 10^5$, $D_t \approx D_p = 1.1$ km (see above) and $P_{NEA} = 1.5 \times 10^{-17}$ km^{-2} yr^{-1} (Bottke et al. 1994), we find $\tau_{col} \gtrsim 10^{11}$ yr. This is much longer than $\tau_{sync} = 10^{4-5}$ yr (Fang & Margot 2012) and the mean dynamical lifetime of NEAs $\sim 10^6$ yr (Bottke et al. 2002; Morbidelli et al. 2002), suggesting the absence of a catastrophic event (see Section 4.1).

On the other hand, micrometeorite impacts may result in ejecting the meteoroid-sized particles. The velocity distribution for micrometeorites near Earth, U, is $12 \sim 70 \, \mathrm{km \, s^{-1}}$ (see radar observations; Nesvorný et al. 2010; Janches et al. 2014; Carrillo-Sánchez et al. 2015). For equal target and impactor densities, the ratio of the ejecta mass, m_e, traveling faster than the escape velocity, v_e, to impactor mass, m_i, is related by

$$m_e / m_i = A (v_e / U)^\alpha, \qquad (6)$$

where $A \sim 0.01$, $\alpha \sim -1.5$ (Housen & Holsapple 2011). Substituting $m_e \sim 30 \, \mathrm{g}$ (fireball mass), $v_e = 0.68 \, \mathrm{m \, s^{-1}}$, and $U = 12$–$70 \, \mathrm{km \, s^{-1}}$ into Equation (6), we find that micrometeorite impactors in the size range of $0.4 \, \mathrm{mm} \leqslant a_i \leqslant 1 \, \mathrm{mm}$ ($m_i = (0.1$–$1.3) \times 10^{-3} \, \mathrm{g}$ with $\rho = 2.7 \, \mathrm{g \, cm^{-3}}$) can eject the centimeter-sized dust particles. The perpendicular impact strength of $> 10^{11} \, \mathrm{N \, m^{-2}}$ is estimated from the equation of impact force per unit area given by $m_i U / \delta t \times 4 / \pi \, a_i^2$, where $\delta t = a_i / U$ is the assumed extend impact time (s). The value is by orders stronger than the compressive strengths of stone meteorites, $\sim 10^8 \, \mathrm{N \, m^{-2}}$ (Flynn et al. 2018), suggesting that micrometeorites are certainly smashing the surface. In this case, many of unknown relevant physical parameters (e.g., impact frequency, population of micrometeorite near 2003 YT$_1$) prevent exact estimation, however, offer probable insight for dust production.

4.2.4. Thermal Fracture

Thermal fracture and fatigue of the asteroid surfaces can be caused by desiccation stress, with the release of dust particles (Jewitt & Li 2010). For 2003 YT$_1$, the peak perihelion temperature, $T_q \sim 440 \, \mathrm{K}$, is about half or less of those of near-Sun asteroids (see Phaethon; Jewitt 2013), while the thermal stress $\lesssim 50 \, \mathrm{MPa}$ is somewhat responsible for the breakdown of the rocky surfaces of most asteroids in the inner solar system (Figure 9(b) in Molaro et al. 2015). The characteristic speeds of dust particles produced by thermal disintegration can be computed by conversion from thermal strain energy into kinetic energy of ejected dust particles. We use the required conversion efficiency, η, given by (see Equation (3) of Jewitt & Li 2010)

$$\eta \sim \left(\frac{v_e}{\alpha \, \delta T} \right)^2 \left(\frac{\rho}{Y} \right), \qquad (7)$$

where again $v_e = 0.68 \, \mathrm{m \, s^{-1}}$, $\alpha \sim 10^{-5} \, \mathrm{K^{-1}}$ is the characteristic thermal expansivity of rock (Lauriello 1974; Richter & Simmons 1974), $\delta T \sim 80 \, \mathrm{K}$ is the temperature variation between the q and aphelion, and $Y = (1$–$10) \times 10^{10} \, \mathrm{N \, m^{-2}}$ are Young's moduli for rock in general (Pariseau 2006). With ρ as above we find $\eta \gtrsim 2\%$–20% is needed for the velocities of ejected dust particles to surpass the escape velocity. The value of conversion efficiency is small enough for most dust particles to be launched into interplanetary space.

Note that micron-sized particles are observed from the Phaethon tails at perihelion, possibly produced by a combination of thermal fracture and radiation pressure (Jewitt et al. 2013; Hui & Li 2017). Such tiny particles are distinct from the millimeter–centimeter scale dust. Larger, mass-dominant particles could be launched, but the acquisition of more and better data for estimation is needed (Jewitt et al. 2018, 2019a). This mechanism is hence pending.

4.2.5. Photoionization

Photoionization by solar UV induces electrostatic forces to eject very small particles. For a 1 km diameter asteroid, 2003 YT$_1$, the critical size is estimated to be $a_e \lesssim 4 \, \mu\mathrm{m}$ (Equation (12) of Jewitt et al. 2015). Therefore, millimeter–centimeter scale particles cannot be launched. We conclude that this process is improbable.

4.2.6. Radiation Pressure Sweeping

Small dust particles on the surface of asteroids, if they briefly lose contact forces, can be stripped away by radiation pressure sweeping. By equating the net surface acceleration (gravitational and centripetal) with the acceleration due to radiation pressure, we estimate the critical size to be swept away, a_{rad} ($\mu\mathrm{m}$), with Equation (6) of Jewitt & Li (2010),

$$a_{\mathrm{rad}} \sim \frac{3 \, g_\odot}{2 \, \pi \, R_{\mathrm{au}}^2 \, f^{1/2} \, D_e} \left[\frac{G \, \rho}{f^2} - \frac{3 \, \pi}{P_{\mathrm{rot}}^2} \right]^{-1}, \qquad (8)$$

where $g_\odot$ is the gravitational acceleration to the Sun at 1 au, R_{au} is the heliocentric distance expressed in astronomical units, f is the limit to the axis ratio ($= a / b$), and G is the gravitational constant. We substitute $g_\odot = 0.006 \, \mathrm{m \, s^{-2}}$, $R_{\mathrm{au}} = 0.786$ (non-dimensional), and adopt the same values of f, G, $D_e (= D_p)$, ρ, and P_{rot} (as applied so far) into Equation (8), then we obtain $a_{\mathrm{rad}} \sim 2900 \, \mu\mathrm{m} \approx 3 \, \mathrm{mm}$. The millimeter-sized dust particles can be swept by radiation pressure from 2003 YT$_1$, which could be the source of meteors. Even if they arrived at Earth, the relatively small size and slow velocity would produce meteors of $m_{\mathrm{obs}} \sim +5 \, \mathrm{mag}$ (Table 1 in Lindblad 1987), being too faint for most optical surveys. By contrast, the centimeter-sized dust particles (source of fireballs) are unlikely to be released.

4.2.7. Sublimation of Water Ice

Sublimation of water ice may be an improbable dust production mechanism for differentiated (V-type) or thermally metamorphosed (S-type) asteroids. On the contrary, the presence of aqueously altered minerals on those of surfaces have been reported (Rivkin et al. 2015, 2018), as well as further evidence such as the weakly active S-type Oort Cloud object driven by the sublimation of water ice (Meech et al. 2016) and the native water inclusion in Itokawa samples (Jin & Bose 2019). Asteroid (4) Vesta's current surface texture, fracture, and roughness (1 cm to 10 cm scale) could be caused by (carbonaceous) impactors (Hasegawa et al. 2003; De Sanctis et al. 2012; Russell et al. 2013, 2015). By contrast, the recent Dawn bistatic radar observation indicates subsurface volatile (water ice) involvement processes (Palmer et al. 2017).

Can buried water ice exist and survive even in V-type asteroids? The differentiation process would occur for the most part of the body, but partially may not. The Vesta's smoother terrain area (heightened hydrogen $> 0.015\%$), on which subsurface ice might contribute to, occupies only $\gtrsim 0.01\%$ of the total surface area (Palmer et al. 2017). The extreme partiality might lead to the localized subsurface ice existence.

How deep can water ice survive in the 2003 YT$_1$ primary, if it were therein? Megaregolith-like materials (large, rubble, brecciated bedrock), with similar structure as found in Vesta (Denevi et al. 2012; Hoffmann et al. 2012), have low thermal

diffusivity of $\kappa \sim 10^{-7} - 10^{-8}$ m^2 s^{-1} (Haack et al. 1990; Fu et al. 2014). The diurnal thermal skin depth (at which the temperature is reduced to be a factor of $1/e$), d_s, is estimated by $\sim \sqrt{\kappa P_{rot}}$. Setting $\kappa = 10^{-7} - 10^{-8}$ m^2 s^{-1} and $P_{rot} = 2.343$ hr we find $d_s \sim 0.9$–3 cm. The blackbody temperature at the thermal skin depth is ~ 120 K even at perihelion, below the sublimation temperature of water ice of 150 K (Yamamoto 1985). Conceivably, water ice might be preserved in the very shallow subsurface within a few centimeters.

To estimate the size of ejected dust particles coupled to the outflowing gas driven by the sublimation of water ice, the small source approximation (SSA) model is applied (Jewitt et al. 2014b). We assume a small patch of surface water ice on 2003 YT$_1$, and also assume that subsurface water ice acts in a similar way to the exposed ice. Spacecraft visits to comets find too small of ice exposure on the nuclei (67P/C-G; Hu et al. 2017) to explain the measured activities driven by sublimation on which a few ~ 10s of percent of surface ice coverages are presumed to replenish (Tancredi et al. 2006). Alternatively, shallow subsurface water ice is proposed as having the most contribution (67P and Ceres; Agarwal et al. 2017; Küppers 2019). A non-rotating, spherical object is assumed for the physical essence of gas dynamics. This prevents complicated gas flows caused by the inhomogeneous distribution of gas release from the non-spherical object (Fulle et al. 2015; Agarwal et al. 2016). Then, ice sublimation from an exposed ($\approx$subsurface) ice patch located at the subsolar point is examined. We solved the energy balance equation of a completely absorbing (sub)surface ice at the subsolar point, with 2003 YT$_1$ located at perihelion $q = 0.786$ au. The subsolar temperature at the d_s is ~ 160 K, warm enough for water ice to sublimate. The flux energy completely absorbed from the Sun and energy lost from the asteroid surface by radiation and latent heat of ice sublimation are calculated. The resulting maximum specific mass-loss rate is $(dm/dt)_{ice} = 8 \times 10^{-4}$ kg m^{-2} s^{-1} at the subsolar point (at the highest temperature of 206 K of the non-rotating body). The terminal velocity in the SSA by gas drag is very small compared to the gravitational escape speed from the asteroid, but certainly assists in launching dust particles from the surface into interplanetary space. The radius of the ice sublimating area (patch), r_{ice}, is related with the critical size of dust particles to be ejected, a_c, as expressed by Equation (A6) of Jewitt et al. (2014b),

$$r_{ice} > \frac{8\pi G \rho^2 D_p^2 a_c}{9 C_D v_{gas}} \left(\frac{dm}{dt} \right)_{ice}^{-1}, \tag{9}$$

where $C_D \sim 1$ is a dimensionless drag coefficient that depends on the shape and nature of the grain and v_{gas} is the thermal speed of gas molecules. We set $a_c = 1$ mm–1 cm using $v_{gas} = 490$ m s^{-1} (Equation (10) of Graykowski & Jewitt 2019) and $(dm/dt)_{ice} = 8 \times 10^{-4}$ kg m^{-2} s^{-1} and again take the same values of G, ρ, and D_p. We then find $r_{ice} > 3$–25 m corresponding to the fractional area of (sub)surface ice of $\sim 0.001\%$–0.05%. This value is 10 times smaller than, or comparable with, those of Vesta ($\gtrsim 0.01\%$; Palmer et al. 2017) and the S-type Oort Cloud object (0.04%–0.1%; Meech et al. 2016). These give a crude but useful estimation, by showing that even a tiny (sub)surface ice coverage can release the meteoroid-sized particles. Yet note that no exposed water ice is observed on 2003 YT$_1$. Note also that it is difficult to detect

subsurface ice by observations. Laboratory data find that even a few millimeter thick crust (organic mantle) perfectly attenuates the near-infrared absorption band depths of the subsurface water ice (Poch et al. 2016). Spacecraft missions for excavations like NASA's Deep Impact (A'Hearn et al. 2005; Kasuga et al. 2006, 2007) and JAXA's Hayabusa2 (Watanabe et al. 2017) would be advantageous for the detection in the kilometer-scale NEAs. Until then the sublimation of water ice, at least, remains as a potential dust production mechanism for 2003 YT$_1$.

Briefly we have examined a variety of processes capable of launching dust particles from 2003 YT$_1$. Rotational instability, impacts, and radiation pressure can produce millimeter to centimeter scale dust particles. By contrast, resurfacing and photoionization are implausible. Insufficient evidence exists in the thermal fracture and sublimation of ice, requiring future work.

5. Summary

We present the SonotaCo meteor survey of a fireball taken in Japan on UT 2017 April 28 at $15^h 58^m 19^s$. The data is measured for orbit and physical properties. Specific detections give the following results.

1. Radiant point, geocentric velocity, and orbital elements of the fireball are determined. The similarity to asteroid 2003 YT$_1$ with D-criterions (see $D_{SH} = 0.0079$) gives an order of smaller values than the significant threshold, indicating a parental association.
2. The absolute visual magnitude is $M_v = -4.10 \pm 0.42$ mag. Light curves give the meteoroid mass of $m = 29 \pm 1$ g, which corresponds to the size $a_s = 2.7 \pm 0.1$ cm with the density of 2700 kg m^{-3}.
3. The meteor luminous model comprising time derivative of momentum in the drag equation is suggested to employ a velocity-dependent ablation coefficient, as determined by $\sigma v^2 < 1$.
4. The 2003 YT$_1$ binary could be rotationally disrupted asteroids with mass shedding, consistent with Pravec & Harris (2007). The YORP spin-up timescale is $\tau_Y \sim 2$ Myr, which shortly induces rotational instability. The resulting end-state is a breakup/fission if it is the rubble-piled body held by a weak cohesive strength of $S_c \sim 240$ N m^{-2}.
5. Micrometeorite impactors with $\simeq 1$ mm in size sufficiently produce the centimeter-sized dust particles, given that they populated near the 2003 YT$_1$ orbit.
6. Radiation pressure may sweep out the millimeter-sized particles from 2003 YT$_1$, which could be the source of faint meteors with an apparent magnitude of $\sim +5$ mag. The centimeter-sized particles are too large to be removed.
7. The other dust production mechanisms are unprovable or pending.

presentation source and to Daniel J. Scheeres as the scientific editor. Finally, we express a deep gratitude to Juraj Tóth and his local organizing committee (LOC) members of Meteoroids 2019 held in Bratislava, Slovakia for providing the opportunity to enhance this study.

Software: UFOCaptureHD2, UFOOrbitV2, UFOAnalyzerV2 (SonotaCo 2009, 2016, 2017; SonotaCo et al. 2014).

Appendix A
Meteor Search in SonotaCo and EDMOND Databases

We used the SonotaCo and EDMOND databases to find other probable meteors that could be orbitally associated with asteroid 2003 YT$_1$ and the Kyoto fireball. Note that slow-speed

meteors infer large uncertainties in the radiant points (Sato & Watanabe 2014; Tsuchiya et al. 2017), while the databases include little or nothing about estimations for errors on orbital information. Hence based on the asteroidal solar longitudes and radiant points in Table 2, we set the wide search ranges of $\lambda_s - 30° \leqslant \lambda_s' \leqslant \lambda_s + 30°$, $\alpha - 30° \leqslant \alpha' \leqslant \alpha + 30°$, $\delta - 20° \leqslant \delta' \leqslant \delta + 20°$ and $v_g < 35\,\mathrm{km\,s^{-1}}$ at the descending or ascending node, respectively. In which λ_s', α', and δ' are those of meteors in the databases. Among them we take any of the *D*-criterion for either the asteroid or the fireball that presents the value of <0.2. Selected meteors are shown in Tables 8 and 9. The scattered results may not be sufficient to be part of the association.

Table 8
Meteor Search in SonotaCo Network and EDMOND Databases

Data No.	UT[a]	λ_s[b] (deg)	α[c] (deg)	δ[d] (deg)	v_g[e] ($\mathrm{km\,s^{-1}}$)	a[f] (au)	e[g]	i[h] (deg)	q[i] (au)	ω[j] (deg)	Ω[k] (deg)
Descending Node											
SonotaCo											
1	2010 Apr 16 18:08:41	26.5027	305.10	36.25	33.6	1.079	0.296	66.8	0.759	86.2	26.503
2	2011 May 8 15:25:36	47.5478	307.11	39.91	17.5	0.774	0.312	36.1	0.533	9.9	47.548
3	2013 Apr 22 18:45:38	32.6091	331.27	44.57	19.2	0.957	0.355	33.5	0.617	61.7	32.609
4	2013 May 13 16:58:56	52.9028	303.43	63.69	23.8	1.544	0.364	42.7	0.982	153.3	52.903
5	2015 May 9 18:45:44	48.6164	309.12	60.33	25.2	1.467	0.347	45.5	0.957	143.0	48.616
EDMOND											
6	2007 Apr 28 00:21:33	37.2620	337.63	43.36	26.1	1.110	0.481	44.9	0.576	71.6	37.262
7	2008 Apr 14 22:01:17	25.2108	305.02	38.83	29.0	0.998	0.272	57.5	0.726	73.1	25.211
8	2008 May 7 00:33:43	46.7232	339.21	44.20	27.2	1.020	0.463	49.8	0.548	63.6	46.723
9	2009 Apr 11 23:19:58	22.0683	322.24	46.81	17.3	1.008	0.287	30.3	0.719	74.5	22.069
10	2009 Apr 22 00:20:56	31.8898	301.19	45.25	31.6	1.317	0.291	59.9	0.934	133.2	31.890
11	2009 May 11 23:44:06	51.2722	305.20	52.71	29.1	1.360	0.278	54.8	0.982	150.6	51.272
12	2010 Apr 8 22:38:54	18.8401	339.18	53.61	17.2	1.381	0.401	26.2	0.827	113.0	18.840
13	2011 Apr 23 20:30:16	33.1847	314.67	42.29	27.8	1.019	0.312	54.0	0.701	74.2	33.185
14	2011 May 3 22:57:34	43.0077	337.37	49.87	25.8	1.194	0.432	45.2	0.678	85.1	43.008
15	2011 May 6 20:32:49	45.8181	302.83	55.76	24.5	1.255	0.227	46.0	0.970	142.4	45.818
16	2011 May 9 00:37:59	47.9189	308.65	47.90	32.7	1.355	0.295	62.2	0.956	140.0	47.919
17	2012 Apr 26 02:49:16	36.1120	312.80	41.43	34.7	1.284	0.364	66.6	0.817	107.2	36.112
18	2014 Apr 24 00:56:19	33.5844	302.11	41.38	21.0	0.846	0.234	42.9	0.648	28.7	33.584
19	2015 Apr 24 03:20:15	33.4362	325.77	47.71	22.8	1.065	0.344	41.1	0.699	79.0	33.436
20	2016 Apr 30 21:09:05	40.7152	321.69	46.50	31.1	1.267	0.392	58.1	0.771	99.5	40.715
Ascending Node											
SonotaCo											
21	2008 Oct 20 18:57:59	207.6334	73.36	−33.07	22.8	1.065	0.357	40.5	0.685	100.7	27.634
22	2011 Oct 26 16:20:31	212.7369	76.86	−34.25	22.2	1.076	0.336	39.4	0.715	96.8	32.737

Notes. From SonotaCo Network Data Sets (http://sonotaco.jp/doc/SNM/index.html) in 2007–2018 and EDMOND Database (https://www.meteornews.net/edmond/edmond/edmond-database/) in 2001–2016.
[a] Observed date and time.
[b] Solar longitude (J2000.0).
[c] R.A. (J2000.0).
[d] Decl. (J2000.0).
[e] Geocentric velocity.
[f] Semimajor axis.
[g] Eccentricity.
[h] Inclination.
[i] Perihelion distance.
[j] Argument of perihelion.
[k] Longitude of ascending node.

Table 9
D-criterions for Searched Meteors

Data No.	2003 YT$_1$			Fireball		
	$D_{\rm SH}$ [a]	D' [b]	$D_{\rm ACS}$ [c]	$D_{\rm SH}$ [a]	D' [b]	$D_{\rm ACS}$ [c]
Descending Node						
SonotaCo						
1	0.436	0.177	0.394	0.439	0.178	0.397
2	0.469	0.260	0.180	0.468	0.257	0.177
3	0.329	0.243	0.202	0.325	0.239	0.197
4	0.491	0.212	0.163	0.494	0.210	0.160
5	0.397	0.173	0.133	0.401	0.171	0.132
EDMOND						
6	0.315	0.348	0.190	0.310	0.342	0.185
7	0.334	0.159	0.237	0.337	0.162	0.241
8	0.350	0.346	0.200	0.346	0.340	0.198
9	0.342	0.191	0.243	0.340	0.192	0.239
10	0.370	0.142	0.283	0.375	0.145	0.287
11	0.465	0.177	0.205	0.470	0.181	0.208
12	0.382	0.201	0.342	0.378	0.195	0.337
13	0.235	0.162	0.176	0.236	0.161	0.179
14	0.187	0.277	0.144	0.181	0.271	0.140
15	0.336	0.185	0.088	0.341	0.193	0.092
16	0.477	0.174	0.325	0.482	0.177	0.328
17	0.407	0.175	0.401	0.410	0.171	0.403
18	0.332	0.195	0.107	0.334	0.199	0.110
19	0.158	0.195	0.075	0.154	0.192	0.070
20	0.274	0.169	0.269	0.275	0.163	0.270
Ascending Node						
SonotaCo						
21	0.185	0.130	0.092	0.179	0.121	0.086
22	0.134	0.091	0.094	0.127	0.083	0.088

Notes. Significance is set to $D < 0.20$ (Williams et al. 2019).
[a] Southworth & Hawkins (1963).
[b] Drummond (1981).
[c] Asher et al. (1993).

Appendix B
Meteor Luminous Model

We present a procedure to develop a new meteor luminous model based on the classical model (Bronshten 1983; Ceplecha et al. 1998; reviewed in Popova et al. 2019). The meteoroid kinetic energy is transformed into radiation during the meteor flight. The classical luminous model equating mass loss (ablation), luminosity, and deceleration is given by (Chapter 3.4 in Ceplecha et al. 1998)

$$I = -\tau \frac{d}{dt}\left(\frac{mv^2}{2}\right)$$
$$= -\tau\left(\frac{v^2}{2}\frac{dm}{dt} + mv\frac{dv}{dt}\right) \quad (10)$$
$$= -\tau\left(1 + \frac{2}{\sigma v^2}\right)\frac{v^2}{2}\frac{dm}{dt}, \quad (11)$$

where I is the meteor luminosity, τ is the luminous efficiency, m is the meteoroid mass (g), σ is the ablation coefficient ($\rm s^2\,km^{-2}$) ($=\rm kg\,MJ^{-1}$), v is the meteor velocity ($\rm cm\,s^{-1}$), and t (s) is time. The meteor luminosity is defined as $I = 10^{-0.4M_{\rm v}}$ in magnitude-based units in the visual region, where $M_{\rm v}$ is the absolute magnitude in the 100 km distance. The ablation coefficient is generally defined as $\sigma = \Lambda/2Q\Gamma$, where Λ is the heat transfer

coefficient, Q is the energy necessary to ablate an unit mass of meteoroid ($\rm MJ\,kg^{-1}$), and Γ is the drag coefficient. The motion and ablation of a single non-fragmenting body through the atmosphere has been traditionally represented by the drag and mass-loss equations as (Chapter 3.2 in Ceplecha et al. 1998)

$$m\frac{dv}{dt} = -\Gamma S\rho_{\rm a}v^2, \quad (12)$$

$$\frac{dm}{dt} = -\frac{\Lambda S}{2Q}\rho_{\rm a}v^3, \quad (13)$$

respectively. Here S is the cross-section of meteoroid and $\rho_{\rm a}$ is the atmospheric density. The Equations (12) and (13) are related as

$$\frac{dv}{dt} = \frac{1}{\sigma mv}\frac{dm}{dt}. \quad (14)$$

Substituting Equation (14) into (10), we obtain the classical luminous model in Equation (11).

A new luminous model is developed by refining the drag in Equation (12). Since the ablation process can lose the mass of meteoroid itself, the drag force should be expressed in the differential form of the momentum (Nagasawa 1981, in Japanese). The drag in Equation (12) thus can be rewritten as

$$\frac{d}{dt}(mv) = m\frac{dv}{dt} + \frac{dm}{dt}v = -\Gamma S\rho_{\rm a}v^2. \quad (15)$$

Substituting Equation (13) into (15), the refined drag equation is obtained as

$$m\frac{dv}{dt} = -\Gamma S\rho_{\rm a}v^2(1 - \sigma v^2), \quad (16)$$

where $\sigma v^2 < 1$ is required. The new relation between dv/dt and dm/dt using Equations (13) and (16) finds

$$\frac{dv}{dt} = \frac{1 - \sigma v^2}{\sigma mv}\frac{dm}{dt}. \quad (17)$$

By substituting Equation (17) into (10), we obtain the new luminous model,

$$I = -\tau\left(\frac{2}{\sigma v^2} - 1\right)\frac{v^2}{2}\frac{dm}{dt}. \quad (18)$$

The ablation coefficient, σ, characterizes the ability of a meteoroid to ablate. A larger value produces higher mass-loss, resulting in brighter luminosity. The estimated values in the published literature are, however, highly scattered and inconclusive. The distribution of a coefficient (single-body theory) showing $0.01 < \sigma < 0.6\,\rm s^2\,km^{-2}$ is used to classify the meteoroid type, such as ordinary ($0.014\,\rm s^2\,km^{-2}$), carbonaceous chondrites ($0.042\,\rm s^2\,km^{-2}$), or soft cometary materials ($0.21\,\rm s^2\,km^{-2}$) and so on (Ceplecha et al. 1993). Later, on the contrary, a fragmentation process is suggested to be dominant for mass loss, finding the low $\sigma = 0.004$–$0.008\,\rm s^2\,km^{-2}$ in any type of meteorite (Ceplecha & Revelle 2005). But the process also depends on the assumed models. The works are reviewed in more detail by Popova et al. (2019).

Here, we propose an appropriate ablation coefficient for the new luminous model therein. It concisely depends on meteor velocity, as determined by $\sigma v^2 < 1$ (see Equation (16)). Setting $v = 23.7\,\rm km\,s^{-1}$ (fireball) finds $\sigma < 0.00178\,\rm s^2\,km^{-2}$. We thus use $\sigma = 0.0017\,\rm s^2\,km^{-2}$ for this study (see Section 3.2).

ORCID iDs

Toshihiro Kasuga ⬤ https://orcid.org/0000-0001-5903-7391
Jun-ichi Watanabe ⬤ https://orcid.org/0000-0003-4391-4446

References

Abell, P. A., Gaffey, M. J., & Hardersen, P. S. 2004, BAAS, 36, 1132
Abell, P. A., Gaffey, M. J., Hardersen, P. S., et al. 2005, BAAS, 37, 627
Agarwal, J., A'Hearn, M. F., Vincent, J. B., et al. 2016, MNRAS, 462, S78
Agarwal, J., Della Corte, V., Feldman, P. D., et al. 2017, MNRAS, 469, s606
Agarwal, J., Jewitt, D., & Weaver, H. 2013, ApJ, 769, 46
A'Hearn, M. F., Belton, M. J. S., Delamere, W. A., et al. 2005, Sci, 310, 258
Asher, D. J., Clube, S. V. M, & Steel, D. I. 1993, MNRAS, 264, 93
Binzel, R. P., Morbidelli, A., Merouane, S., et al. 2010, Natur, 463, 331
Bottke, W. F., Morbidelli, A., Jedicke, R., et al. 2002, Icar, 156, 399
Bottke, W. F. J., Nolan, M. C., Greenberg, R., & Kolvoord, R. A. 1994, in
    Hazards due to Comets and Asteroids, ed. T. Gehrels, M. S. Matthews, &
    A. M. Schumann (Tucson, AZ: Univ. Arizona Press), 337
Bronshten, V. A. 1983, Physics of Meteoric Phenomena (Dordrecht: Reidel)
Brooks, H. E. 2006, BAAS, 38, 934
Brown, P., Marchenko, V., Moser, D. E., Weryk, R., & Cooke, W. 2013,
    M&PS, 48, 270
Burbine, T. H., Buchanan, P. C., Dolkar, T., & Binzel, R. P. 2009, M&PS,
    44, 1331
Carrillo-Sánchez, J. D., Plane, J. M. C., Feng, W., Nesvorný, D., & Janches, D.
    2015, GeoRL, 42, 6518
Ceplecha, Z., Borovička, J., Elford, W. G., et al. 1998, SSRv, 84, 327
Ceplecha, Z., & McCrosky, R. E. 1976, JGR, 81, 6257
Ceplecha, Z., & Revelle, D. O. 2005, M&PS, 40, 35
Ceplecha, Z., Spurny, P., Borovicka, J., & Keclikova, J. 1993, A&A, 279, 615
Chandler, C. O., Kueny, J., Gustafsson, A., et al. 2019, ApJL, 877, L12
Chang, C.-K., Ip, W.-H., Lin, H.-W., et al. 2015, ApJS, 219, 27
Clark, D. L., Wiegert, P., & Brown, P. G. 2019, MNRAS, 487, L35
Cochran, A. L., Vilas, F., Jarvis, K. S., & Kelley, M. S. 2004, Icar, 167, 360
Cruikshank, D. P., Tholen, D. J., Hartmann, W. K., Bell, J. F., & Brown, R. H.
    1991, Icar, 89, 1
Davis, D. R., Durda, D. D., Marzari, F., Campo Bagatin, A., & Gil-Hutton, R.
    2002, in Asteroids III, ed. W. F. Bottke, Jr. et al. (Tucson: Univ. Arizona
    Press), 545
De Sanctis, M. C., Combe, J. P., Ammannito, E., et al. 2012, ApJL, 758, L36
Delbo, M., Walsh, K., Mueller, M., Harris, A. W., & Howell, E. S. 2011, Icar,
    212, 138
Denevi, B. W., Coman, E. I., Blewett, D. T., et al. 2012, LPSC, 1659, 1943
Drummond, J. D. 1981, Icar, 45, 545
Dumitru, B. A., Birlan, M., Popescu, M., & Nedelcu, D. A. 2017, A&A,
    607, A5
Fang, J., & Margot, J.-L. 2012, AJ, 143, 24
Flynn, G. J., Consolmagno, G. J., Brown, P., & Macke, R. J. 2018, ChEG,
    78, 269
Flynn, G. J., & Durda, D. D. 2004, P&SS, 52, 1129
Fu, R. R., Hager, B. H., Ermakov, A. I., & Zuber, M. T. 2014, Icar, 240, 133
Fulle, M., Ivanovski, S. L., Bertini, I., et al. 2015, A&A, 583, A14
Fulvio, D., Perna, D., Ieva, S., et al. 2016, MNRAS, 455, 584
Galád, A., Gajdoš, S., Kornoš, L., Vilagi, J., & Pravec, P. 2004, IAUC, 8336, 4
Galiazzo, M. A., Silber, E. A., & Bancelin, D. 2017, AN, 338, 375
Goldreich, P., & Sari, R. 2009, ApJ, 691, 54
Graves, K. J., Minton, D. A., Hirabayashi, M., DeMeo, F. E., & Carry, B.
    2018, Icar, 304, 162
Graves, K. J., Minton, D. A., Molaro, J. L., & Hirabayashi, M. 2019, Icar,
    322, 1
Graykowski, A., & Jewitt, D. 2019, AJ, 158, 112
Haack, H., Rasmussen, K. L., & Warren, P. H. 1990, JGR, 95, 5111
Hasegawa, S., Murakawa, K., Ishiguro, M., et al. 2003, GeoRL, 30, 2123
Hicks, M., Somers, J., Barajas, T., et al. 2009, ATel, 2289, 1
Hirabayashi, M., Scheeres, D. J., Sánchez, D. P., & Gabriel, T. 2014, ApJL,
    789, L12
Hoffmann, M., Nathues, A., Vincent, J. B., & Sierks, H. 2012, EGU General
    Assembly Conf. Abstracts, 14, 5530
Housen, K. R., & Holsapple, K. A. 2011, Icar, 211, 856
Hu, X., Shi, X., Sierks, H., et al. 2017, MNRAS, 469, S295
Hui, M.-T., Kim, Y., & Gao, X. 2019, MNRAS, 488, L143
Hui, M.-T., & Li, J. 2017, AJ, 153, 23
Ieva, S., Dotto, E., Lazzaro, D., et al. 2016, MNRAS, 455, 2871
Jacobson, S. A., & Scheeres, D. J. 2011, ApJL, 736, L19

Janches, D., Plane, J. M. C., Nesvorný, D., et al. 2014, ApJ, 796, 41
Jeffers, S. V., Manley, S. P., Bailey, M. E., & Asher, D. J. 2001, MNRAS,
    327, 126
Jenniskens, P. 2017, P&SS, 143, 116
Jenniskens, P., & Lyytinen, E. 2005, AJ, 130, 1286
Jewitt, D. 2012, AJ, 143, 66
Jewitt, D. 2013, AJ, 145, 133
Jewitt, D., Agarwal, J., Li, J., et al. 2014a, ApJL, 784, L8
Jewitt, D., Agarwal, J., Li, J., et al. 2017, AJ, 153, 223
Jewitt, D., Asmus, D., Yang, B., & Li, J. 2019a, AJ, 157, 193
Jewitt, D., Hsieh, H., & Agarwal, J. 2015, in Asteroids IV, ed. P. Michel,
    F. E. DeMeo, & W. F. Bottke (Tucson, AZ: Univ. Arizona Press), 221
Jewitt, D., Ishiguro, M., & Agarwal, J. 2013, ApJL, 764, L5
Jewitt, D., Ishiguro, M., Weaver, H., et al. 2014b, AJ, 147, 117
Jewitt, D., Kim, Y., Luu, J., et al. 2019b, ApJL, 876, L19
Jewitt, D., & Li, J. 2010, AJ, 140, 1519
Jewitt, D., Mutchler, M., Agarwal, J., & Li, J. 2018, AJ, 156, 238
Jewitt, D., Weaver, H., Agarwal, J., Mutchler, M., & Drahus, M. 2010, Natur,
    467, 817
Jin, Z., & Bose, M. 2019, SciA, 5, eaav8106
Jutzi, M., Michel, P., Benz, W., & Richardson, D. C. 2010, Icar, 207, 54
Kasuga, T., & Jewitt, D. 2019, in Meteoroids: Sources of Meteors on Earth and
    Beyond, ed. G. O. Ryabova, D. J. Asher, & M. D. Campbell-Brown
    (Cambridge: Cambridge Univ. Press), 187
Kasuga, T., Sato, M., & Watanabe, J. 2007, AdSpR, 40, 215
Kasuga, T., Watanabe, J.-I., & Sato, M. 2006, MNRAS, 373, 1107
Kleyna, J. T., Hainaut, O. R., Meech, K. J., et al. 2019, ApJL, 874, L20
Kornoš, L., Koukal, J., Piffl, R., & Tóth, J. 2014a, in Proc. Int. Meteor Conf.,
    ed. M. Gyssens, P. Roggemans, & P. Zoladek (Poznan: A.M. University
    Press), 23
Kornoš, L., Matlovič, P., Rudawska, R., et al. 2014b, in Proc. Astronomical
    Conference: The Meteoroids 2013, ed. T. J. Jopek et al. (Poznań: A.M.
    University Press), 225
Küppers, M. 2019, JGRE, 124, 205
Larson, S. M., Grauer, A. D., Beshore, E., et al. 2004, BAAS, 36, 1139
Lauriello, P. 1974, Int. J. Rock Mech. Min. Sci., 11, 75
Lindblad, B. A. 1987, in Proc. Intern. School of Physics: The Evolution of the
    Small Bodies of the Solar System, ed. M. Fulchignoni & L. Kresak
    (Amsterdam: North-Holland Physics Publications), 229
Madiedo, J. M., Trigo-Rodríguez, J. M., Ortiz, J. L., Castro-Tirado, A. J., &
    Cabrera-Caño, J. 2014, MNRAS, 443, 1643
Madiedo, J. M., Trigo-Rodríguez, J. M., Williams, I. P., Ortiz, J. L., &
    Cabrera, J. 2013, MNRAS, 431, 2464
Mainzer, A., Grav, T., Bauer, J., et al. 2011, ApJ, 743, 156
Mainzer, A., Grav, T., Masiero, J., et al. 2012, ApJL, 760, L12
Margot, J. L., Pravec, P., Taylor, P., Carry, B., & Jacobson, S. 2015, in
    Asteroids IV, ed. P. Michel, F. E. DeMeo, & W. F. Bottke (Tucson: Univ.
    Arizona Press), 355
Marsset, M., DeMeo, F., Sonka, A., et al. 2019, ApJL, 882, L2
Meech, K. J., Yang, B., Kleyna, J., et al. 2016, SciA, 2, e1600038
Molaro, J. L., Byrne, S., & Langer, S. A. 2015, JGRE, 120, 255
Morbidelli, A., Bottke, W. F., Froeschlé, C., & Michel, C. 2002, in Asteroids
    III, ed. W. F. Bottke, Jr. et al. (Tucson: Univ. Arizona Press), 409
Moreno, F., Jehin, E., Licandro, J., et al. 2019, A&A, 624, L14
Moskovitz, N. A., Fatka, P., Farnocchia, D., et al. 2019, Icar, 333, 165
Myers, J. R., Sande, C. B., Miller, A. C., Warren, W. H. J., & Tracewell, D. A.
    2001, yCat, V/109, 1
Nagasawa, K. 1981, The Earth Monthly, 3, 588
Neslusan, L., Svoren, J., & Porubcan, V. 1998, A&A, 331, 411
Nesvorný, D., Jenniskens, P., Levison, H. F., et al. 2010, ApJ, 713, 816
Nolan, M. C., Howell, E. S., & Hine, A. A. 2004a, IAUC, 8336, 3
Nolan, M. C., Howell, E. S., & Miranda, G. 2004b, AAS/DPS Meeting,
    36, 28.08
Olech, A., Żołądek, P., Wiśniewski, M., et al. 2017, MNRAS, 469, 2077
Palmer, E. M., Heggy, E., & Kofman, W. 2017, NatCo, 8, 409
Pariseau, G. W. 2006, Design Analysis in Rock Mechanics (London: Taylor
    and Francis)
Pieters, C. M., Ammannito, E., Blewett, D. T., et al. 2012, Natur, 491, 79
Poch, O., Pommerol, A., Jost, B., et al. 2016, Icar, 267, 154
Popova, O., Borovička, J., & Campbell-Brown, M. D. 2019, in Meteoroids:
    Sources of Meteors on Earth and Beyond, ed. G. O. Ryabova,
    D. J. Asher, & M. D. Campbell-Brown (Cambridge: Cambridge Univ.
    Press), 9
Pravec, P. 2005, in Society for Astronomical Sciences Annual Symp. 24, ed.
    B. D. Warner et al. (Rancho Cucamonga, CA: SAS), 61
Pravec, P., & Harris, A. W. 2007, Icar, 190, 250

Pravec, P., Harris, A. W., Vokrouhlický, D., et al. 2008, Icar, 197, 497
Pravec, P., Scheirich, P., Kušnirák, P., et al. 2016, Icar, 267, 267
Richter, D., & Simmons, G. 1974, Int. J. Rock Mech. Min. Sci. Geomech. Abstr., 11, 403
Rivkin, A. S., Campins, H., Emery, J. P., et al. 2015, in Asteroids IV, ed. P. Michel, F. E. DeMeo, & W. F. Bottke (Tucson: Univ. Arizona Press), 65
Rivkin, A. S., Howell, E. S., Emery, J. P., & sunshine, J. 2018, Icar, 304, 74
Rozitis, B., & Green, S. F. 2013, MNRAS, 430, 1376
Rudawska, R., & Jenniskens, P. 2014, in Proc. Astronomical Conference: The Meteoroids 2013, ed. T. J. Jopek et al. (Poznań: A.M. University Press), 217
Russell, C. T., McSween, H. Y., Jaumann, R., & Raymond, C. A. 2015, in Asteroids IV, ed. P. Michel, F. E. DeMeo, & W. F. Bottke (Tucson: Univ. Arizona Press), 419
Russell, C. T., Raymond, C. A., Jaumann, R., et al. 2013, M&PS, 48, 2076
Sanchez, J. A., Michelsen, R., Reddy, V., & Nathues, A. 2013, Icar, 225, 131
Sato, M., & Watanabe, J. 2014, in Proc. Astronomical Conference: The Meteoroids 2013, ed. T. J. Jopek et al. (Poznań: A.M. University Press), 329
Scheeres, D. J., Hartzell, C. M., Sánchez, P., & Swift, M. 2010, Icar, 210, 968
Scheeres, D. J., & Sánchez, P. 2018, PEPS, 5, 25
SonotaCo 2009, JIMO, 37, 55
SonotaCo 2016, JIMO, 44, 42
SonotaCo 2017, JIMO, 45, 95
SonotaCo, Shimoda, C., Inoue, H., Masuzawa, T., & Sato, M. 2014, JIMO, 42, 222
Southworth, R. B., & Hawkins, G. S. 1963, SCoA, 7, 261
Spurný, P., Borovička, J., Mucke, H., & Svoreň, J. 2017, A&A, 605, A68
Subasinghe, D., & Campbell-Brown, M. 2018, AJ, 155, 88
Svetsov, V., Shuvalov, V., Collins, G., & Popova, O. 2019, in Meteoroids: Sources of Meteors on Earth and Beyond, Ryabova, ed. G. O. Ryabova,

D. J. Asher, & M. D. Campbell-Brown (Cambridge: Cambridge Univ. Press), 275
Tancredi, G., Fernández, J. A., Rickman, H., & Licandro, J. 2006, Icar, 182, 527
Tichy, M., Kocer, M., Yeung, W. K. Y., et al. 2003, MPEC, 2003, 2003-Y30
Tsuchiya, C., Sato, M., Watanabe, J.-I., et al. 2017, P&SS, 143, 142
Vaubaillon, J., Neslušan, L., Sekhar, A., Rudawska, R., & Ryabova, G. O. 2019, in Meteoroids: Sources of Meteors on Earth and Beyond, ed. G. O. Ryabova, D. J. Asher, & M. D. Campbell-Brown (Cambridge: Cambridge Univ. Press), 161
Vokrouhlický, D., Bottke, W. F., Chesley, S. R., Scheeres, D. J., & Statler, T. S. 2015, in Asteroids IV, ed. P. Michel, F. E. DeMeo, & W. F. Bottke (Tucson: Univ. Arizona Press), 509
Walsh, K. J., & Jacobson, S. A. 2015, in Asteroids IV, ed. P. Michel, F. E. DeMeo, & W. F. Bottke (Tucson: Univ. Arizona Press), 375
Walsh, K. J., Richardson, D. C., & Michel, P. 2008, Natur, 454, 188
Warner, B., Pravec, P., & Harris, A. P. 2018, Asteroid Lightcurve Database (LCDB) V2.0, urn:nasa:pds:ast-lightcurve-database:2.0, https://sbn.psi.edu/pds/resource/lc.html
Warner, B. D., Harris, A. W., & Pravec, P. 2009, Icar, 202, 134
Watanabe, S.-I., Tsuda, Y., Yoshikawa, M., et al. 2017, SSRv, 208, 3
Weryk, R. J., & Brown, P. G. 2013, P&SS, 81, 32
Williams, I. P., Jopek, T. J., Rudawska, R., Tóth, J., & Kornoš, L. 2019, in Meteoroids: Sources of Meteors on Earth and Beyond, ed. G. O. Ryabova, D. J. Asher, & M. D. Campbell-Brown (Cambridge: Cambridge Univ. Press), 210
Yamamoto, T. 1985, A&A, 142, 31
Ye, Q., Kelley, M. S. P., Bodewits, D., et al. 2019, ApJL, 874, L16
Ye, Q.-Z., Brown, P. G., & Pokorný, P. 2016, MNRAS, 462, 3511